J Nanostruct 15(3): 1253-1267, Summer 2025

RESEARCH PAPER

Adsorptive Removal of Crystal Violet Dye Using Sodium Alginate-g-Poly (Acrylic Acid-Co-Itaconic Acid)/Titanium Dioxide [SA-g-p(AA-IA)/ TiO_2] Hydrogel Nanocomposite

Hussein Abd Al-Hassan [1], Raghad Mohammed Salih [2], Layth S. Jasim [2], Maryam Batool [3]*

[1] Department of Chemistry, College of Science, University of Al-Qadisiyah, Diwaniya 1753, Iraq
[2] Department of Chemistry, College of Education, University of Al-Qadisiyah, Diwaniyah, Iraq
[3] Department of Chemistry, University of Sahiwal, Sahiwal, Pakistan

ARTICLE INFO

Article History:
Received 06 March 2025
Accepted 25 June 2025
Published 01 July 2025

Keywords:
Adsorption
Crystal violet dye
Hydrogel
Nanocomposite
TiO_2

ABSTRACT

The escalating release of synthetic dyes, like crystal violet (CV), into water bodies has triggered significant environmental and health worries due to their toxic nature, stability, and long-lasting presence. This research explores the creation, analysis, and adsorption capabilities of a new sodium alginate-g-poly (acrylic acid-co-itaconic acid)/titanium dioxide [SA-g-p(AA-IA)/TiO_2] hydrogel nanocomposite for effectively eliminating CV dye from water solutions. The composite was produced using free-radical polymerization and underwent detailed characterization *via* FTIR, XRD, and FESEM, confirming the integration of TiO_2 nanoparticles and a highly porous structure. The impact of operational factors such as contact duration, pH level, temperature, initial dye concentration, and the amount of adsorbent used was systematically investigated. The nanocomposite displayed a substantial adsorption capacity of 197.66 mg/g under optimal conditions of pH=10 and reached equilibrium within 90 min. Kinetic analysis demonstrated a strong correlation with the pseudo-second-order model (R^2 = 1), indicating a chemical adsorption mechanism. Adsorption isotherm data aligned with both Langmuir and Freundlich models, suggesting the occurrence of both single-layer and multi-layer adsorption on various surfaces, with a maximum capacity nearing 928 mg/g at 10 °C. Thermodynamic analysis revealed the process to be spontaneous (ΔG = −5.812 kJ/mol) and exothermic (ΔH = −15.737 kJ/mol) with a reduction in system entropy (ΔS = −34.255 J/mol·K). The composite also exhibited notable pH-sensitive swelling behaviour, reaching a maximum of 1155 % at pH=12. These findings highlight the SA-g-p(AA-IA)/TiO_2 nanocomposite as a highly effective adsorbent for removing CV dye from water systems.

How to cite this article
Al-Hassan H., Salih R., Jasim L., Batool M. Adsorptive Removal of Crystal Violet Dye Using Sodium Alginate-g-Poly (Acrylic Acid-Co-Itaconic Acid)/Titanium Dioxide [SA-g-p(AA-IA)/ TiO_2] Hydrogel Nanocomposite . J Nanostruct, 2025; 15(3):1253-1267. DOI: 10.22052/JNS.2025.03.042

INTRODUCTION

The introduction of coloured wastewater from industrial processes into the environment poses a significant and growing threat to the health of aquatic ecosystems. Industries such as textiles, leather finishing, printing, and food production utilize a vast array of synthetic dyes, which are discharged into water bodies without adequate treatment [1]. These dyes, often characterized by complex aromatic structures, exhibit considerable stability and are resistant to biodegradation, leading to their accumulation in aquatic

* *Corresponding Author Email: layth.alhayder@gmail.com*

environments [2, 3]. The presence of these organic pollutants not only detracts from the aesthetic quality of water but also impedes the penetration of sunlight, which is essential for photosynthesis by aquatic plants, thereby disrupting the ecological balance and potentially reducing dissolved oxygen levels [4]. Furthermore, a significant number of dyes and their metabolic byproducts are known to be toxic, carcinogenic, or mutagenic, posing direct risks to aquatic organisms and potentially entering the food chain, with implications for human health [5-7]. Crystal Violet (CV), a dye belonging to the triphenylmethane family, finds widespread application. It serves as a biological stain in both human and animal medicine, a colorant in the textile industry during processing, and contributes a deep violet hue to paints and printing inks and also used in medical field. Despite its diverse applications, CV is recognized as a persistent and environmentally challenging dye molecule that can exert toxic effects. Notably, it functions as a mitotic inhibitor, a potential carcinogen that can promote tumor development in certain fish species [5, 8-11]. Among the various physical and chemical methods available for the removal of dyes from wastewater, adsorption has emerged as a particularly attractive and extensively studied technique [12-14]. This method offers several compelling advantages, including its simplicity of operation, high efficiency in removing dyes even at relatively low concentrations [15-17], cost-effectiveness [18-20], and the potential for the adsorbent material to be regenerated and reused, thereby promoting sustainability [21]. The fundamental principle underlying adsorption involves the transfer of dye molecules from the liquid phase to the surface of a solid adsorbent material, where they are retained through a variety of physical and chemical interactions [22]. These interactions can include electrostatic forces between charged dye molecules and the adsorbent surface, van der Waals forces arising from intermolecular attractions, hydrogen bonding between functional groups on the dye and the adsorbent, and even formation of chemical bonds in the case of chemisorption. The effectiveness of an adsorbent in capturing and retaining dye molecules is determined by its intrinsic properties, as specific surface area, distribution of pore sizes, net surface charge, and presence of functional groups that can interact with the dye molecules [23]. Consequently, a significant focus of research in this field is directed towards development of novel adsorbent materials that possess tailored properties to maximize their dye removal performance. This includes exploring various materials, optimizing their synthesis, and modifying their surface characteristics to enhance affinity for specific types of dyes [23]. The recurring emphasis on the cost-effectiveness and the potential for regeneration of adsorbents underscores the practical viability of adsorption as a sustainable solution for large-scale wastewater treatment applications [23]. Hydrogels, which are three-dimensional networks of hydrophilic polymers capable of absorbing and retaining remarkably large volumes of water or biological fluids relative to their mass, have emerged as a significant class of materials with immense potential for wastewater treatment, particularly in the removal of organic dyes [24]. The inherent physicochemical characteristics, as high porosity, large surface area available for adsorption, modifiable surface chemistry, and significant water retention capacity, make hydrogels excellent candidates for effectively capturing and removing a wide range of pollutants from aqueous solutions [25-27]. Hydrogels can be synthesized from a diverse array of natural polysaccharides, such as sodium alginate (SA), chitosan, cellulose, starch, gellan gum, and guar gum, as well as synthetic polymers, including poly(acrylic acid) (AA), poly(Itaconic acid) (IA) and poly(N-vinyl pyrrolidone) (PNVP) [25, 28, 29]. Polysaccharide-based hydrogels are particularly attractive due to their inherent biocompatibility, biodegradability, low cost, and natural abundance, aligning well with the principles of green chemistry and sustainable development for environmental remediation [30]. Hydrogels creates a vast network structure with a large contact area, facilitating the diffusion of dye molecules into the polymer matrix and enhancing the overall adsorption capacity. Furthermore, the chemical composition and physical structure of hydrogels can be precisely tailored during synthesis to introduce specific functional groups that exhibit a high affinity towards particular classes of dyes, enabling the design of highly selective and efficient adsorbents for targeted pollutant removal [31]. The ongoing research into novel hydrogel synthesis methods, including graft copolymerization, the formation of interpenetrating polymer networks, and the incorporation of various nanomaterials, aims to overcome inherent limitations such as

mechanical strength and adsorption capacity, ultimately paving the way for the development of more efficient and robust hydrogel-based adsorbents for practical applications in wastewater treatment [32]. This investigation focuses on the synthesis and application of a specific hydrogel nanocomposite i.e., sodium alginate-g-poly(acrylic acid-co-Itaconic acid)/titanium dioxide, SA-g-p(AA-IA)/TiO_2. This material is designed to leverage the combined benefits of a natural polysaccharide (sodium alginate), synthetic monomers (acrylic acid and Itaconic acid), and inorganic nanoparticles (titanium dioxide) for the efficient removal of CV dye from aqueous solutions [4]. Sodium alginate, an anionic polysaccharide derived from seaweed, is a readily available, cost-effective, and biodegradable biopolymer that offers a biocompatible matrix for hydrogel formation [33]. The grafting of acrylic acid onto the sodium alginate backbone introduces pH-responsive carboxylic acid functional groups, which can significantly enhance the adsorption of cationic dyes, particularly under alkaline conditions. These groups are deprotonated and exhibit increased electrostatic attraction towards the positively charged dye molecules [34]. The incorporation of itaconic acid, a non-ionic monomer, into the polymer network contributes to the hydrogel's overall structural integrity, mechanical strength, and water swelling capacity, facilitating the accessibility of adsorption sites within the hydrogel matrix [35]. The inclusion of TiO_2 nanoparticles within the hydrogel matrix introduces a component known for its high surface area [36, 37]. The specific objectives of this research include:

i. Synthesizing and thoroughly characterizing the SA-g-p(AA-IA)/TiO_2 hydrogel nanocomposite using appropriate analytical techniques to confirm its successful formation and to understand its structural and morphological properties.

ii. Systematically evaluating the influence of key operational parameters, such as time, pH of solution, temperature, the initial dye concentration, and the dosage of nanocomposite, on efficiency of adsorption process.

iii. Determining the adsorption kinetics by applying established kinetic models, including the pseudo-first-order and pseudo-second-order models, to elucidate the rate-controlling steps and the mechanism of adsorption.

iv. Calculating the thermodynamic parameters, namely the Gibbs free energy change (ΔG), the enthalpy change (ΔH), and the entropy change (ΔS), to assess the spontaneity of adsorption process and to determine whether it is endothermic or exothermic in nature.

v. Analyzing the adsorption equilibrium data using various isotherm models, as Langmuir, Freundlich, and Temkin models, to determine the maximum adsorption capacity of nanocomposite for CV dye and to gain insights into the nature of adsorption mechanism at solid-liquid interface.

A comprehensive investigation of isothermal, kinetics and thermodynamics of CV adsorption on SA-g-p(AA-IA)/TiO_2 nanocomposite will provide a thorough understanding of the adsorption mechanism, enabling the optimization of its performance for efficient and sustainable removal of this dye from wastewater. This knowledge can also contribute for developing more effective hydrogel-based nanocomposite for the removal of a wider range of organic pollutants from contaminated water resources.

MATERIALS AND METHODS

Chemicals

Sodium alginate, with a purity of 99.0 % (Himedia), TiO_2 with 99.7 % purity (Merck). itaconic acid with 99 % purity (Himedia), potassium persulfate with purity of 99 % (Riedel-dehaenag seclze hannover), N, N'-Methylene-bis-Itaconic acid at 99 % purity (Himedia laboratories), ethanol with a purity of 95 % (Merck Energy), acrylic acid at 99 % purity (Himedia), nitrogen gas (Xinrui), sodium hydroxide with 99 % purity (Alpha Chemika), hydrochloric acid at a concentration of 38 % (J.T. Baker), calcium carbonate with 99 % purity (Fluka), potassium chloride at 99.5 % purity (Fluka), CV with 99.0 % (Merck) and tetramethylethylenediamine (TEMED) at 99.0 % purity (Fluka) were used throughout the study.

Preparation SA-g-p(AA-IA)/ TiO_2 hydrogel nanocomposite

The SA-g-p(AA-IA)/TiO_2 hydrogel nanocomposite was synthesized via free-radical copolymerization in an aqueous solution. This involved dissolving 0.12 g of TiO_2 particles in 20 mL of deionized water with continuous stirring for 4 h, followed by transfer to an ultrasonication device for another 4 h. The reaction mixture was then transferred to a three-neck round-bottom flask equipped with a condenser, a dropping funnel, and a nitrogen

gas inlet, placed in a water bath with stirring until complete dissolution was achieved. Subsequently, 0.5 g of sodium alginate (SA) was added portion-wise and slowly to the reaction mixture with stirring for 1 h until a homogeneous solution was obtained. Next, 4 g of acrylic acid (AA) was added portion-wise to the preceding solution with continuous stirring for 15 min. Afterwards, a solution prepared by dissolving 2 g of itaconic acid (IA) in 2 mL of H_2O was added portion-wise to the reaction mixture with continuous stirring for 15 min. Similarly, 0.05 g of N, N'-methylenebisItaconic acid (MBA) (cross-linking agent) was prepared in 2 mL of H_2O and added gradually to solution with stirring for 15 min. Afterwards, four drops of TEMED solution were added with continuous stirring for 5 min. Additionally, a solution of 0.03 g of potassium persulfate (KPS) in 2 mL of H_2O was prepared and added gradually with continuous stirring for 15 min at room temperature under a nitrogen atmosphere via the dropping funnel. The temperature was then raised to 70 °C and maintained for 3 h to complete the polymerization reaction. The synthesized nanocomposite hydrogel SA-g-p(AA-IA)/TiO_2 was immersed in deionized water to remove unreacted monomers. Finally, it was dried in an electric oven at 70 °C to achieve a constant weight.

Adsorption studies and calibration curve

For investigating the potential of synthesized SA-g-p(AA-IA)/ TiO_2 hydrogel nanocomposite as an adsorbent, experiments were conducted in a batch mode for removing CV dye from water. Parameters studied for dye adsorption include time (0-180 min), temperature (10, 15, 20, 30 °C), dye concentration (10-500 mg/L), dose of nanocomposite used (0.001-0.04 g) and pH (2-10). For each experiment, the shaking speed was adjusted to 130 rpm using 10 mL dye solution in a conical flask. For the adjustment of pH, NaOH and HCl, 0.1 M, were used and pH meter was used for pH measurement. After the equilibrium time, the absorbance of solution was measured by using UV-vis spectrophotometer with a λ_{max} of 574 nm. Afterwards, the amount of adsorbed dye on adsorbent surface (mg/g) and % removal of dye were calculated by Eq. 1 and 2 correspondingly [38].

$$q_e = \frac{C_o - C_e * V}{m} \quad (1)$$

$$R\,(\%) = \frac{C_o - C_e}{C_o} \times 100 \quad (2)$$

here, C_o and C_e refers to initial and equilibrium concentrations of CV dye in mg/L, correspondingly while "m" denotes dose of nanocomposite used in "g". The volume of dye solution is represented by V in "L".

The calibration curve for CV dye (Fig. 1),

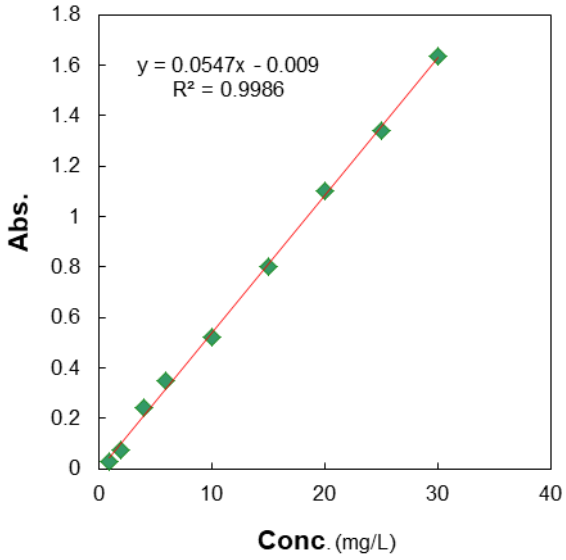

Fig. 1. Calibration curve for CV dye.

established by measuring the absorbance of dye at its maximum absorbance wavelength (around 590-600 nm), demonstrates a strong linear relationship between absorbance and concentration, consistent with Beer-Lambert's law. The resulting linear equation (y = mx + b) with a high coefficient of determination (R^2 = 0.998) provides a reliable tool for quantifying CV dye concentrations in adsorption studies, enabling calculation of residual dye concentration, adsorption capacity, and dye removal efficiency.

RESULTS AND DISCUSSION

Characterization

FTIR analysis of the SA-g-p(AA-IA)/TiO_2 nanocomposite, before and after CV dye adsorption, reveals significant changes in its functional groups. Before dye exposure (Fig. 2), the nanocomposite's spectrum showed characteristic peaks: a broad band at 3300–3400 cm^{-1} for –OH and –NH stretches (from alginate hydroxyls and IA amides), a strong peak at 1650 cm^{-1} for C=O stretching (amide I), and bands near 1550–1600

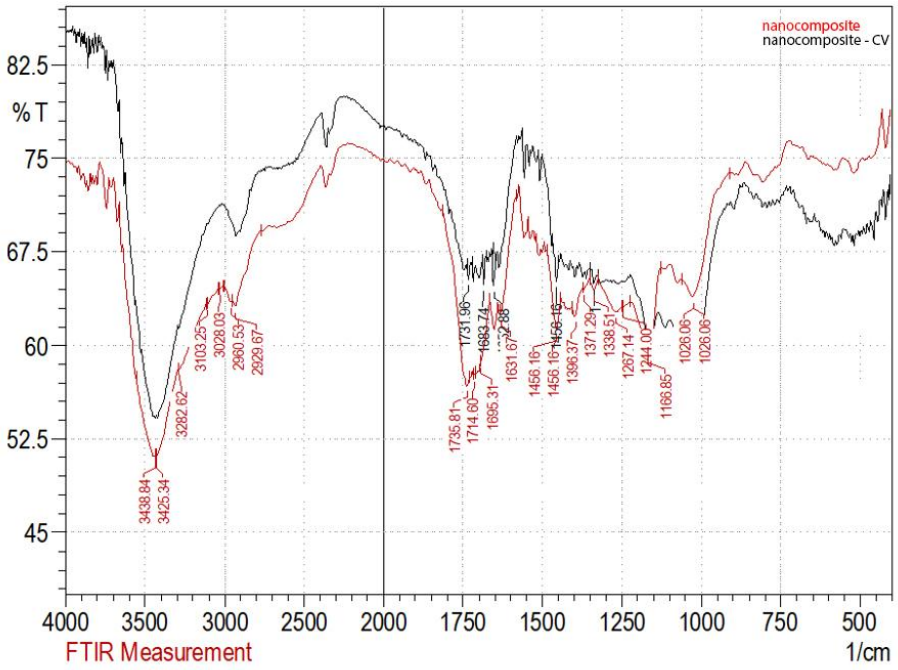

Fig. 2. FTIR of SA-g-p(AA-IA)/ TiO_2 before and after dye adsorption.

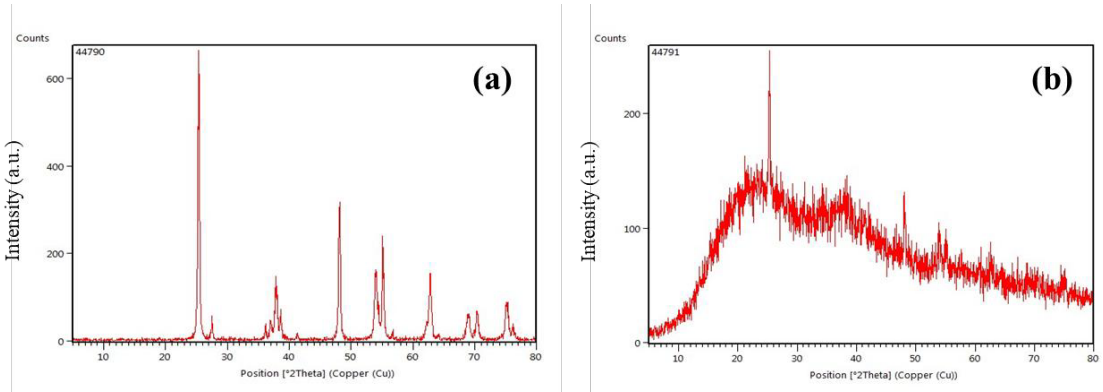

Fig. 3. XRD patterns of (a) TiO_2 and (b) SA-g-p(AA-IA)/TiO_2 nanocomposite.

cm^{-1} (N–H bending/asymmetric $–COO^-$ stretch from AA) and 1400–1450 cm^{-1} (symmetric $–COO^-$ stretch). The C–O–C stretch of polysaccharides appeared around 1020–1080 cm^{-1}, while TiO_2 was confirmed by a band at 500–700 cm^{-1} (Ti–O–Ti vibrations). After CV dye adsorption, noticeable shifts and intensity changes occurred. The –OH/–NH band broadened and shifted, suggesting hydrogen bonding or electrostatic interactions with the dye. The C=O peak at 1650 cm^{-1} showed minor shifts and decreased intensity, indicating interaction with amide or carboxylic acid groups. Shifts or intensity changes near 1550 cm^{-1} point to carboxylate or amine groups involved in electrostatic binding or π–π stacking with the dye's aromatic rings. Changes in the 1400–1450 cm^{-1} regions suggest ionic exchange or electrostatic attraction between the dye's positive charges and the nanocomposite's carboxyl groups. Additionally, the C–O–C peak near 1020–1080 cm^{-1} have changed intensity due to slight polymer backbone rearrangement upon dye binding [39-

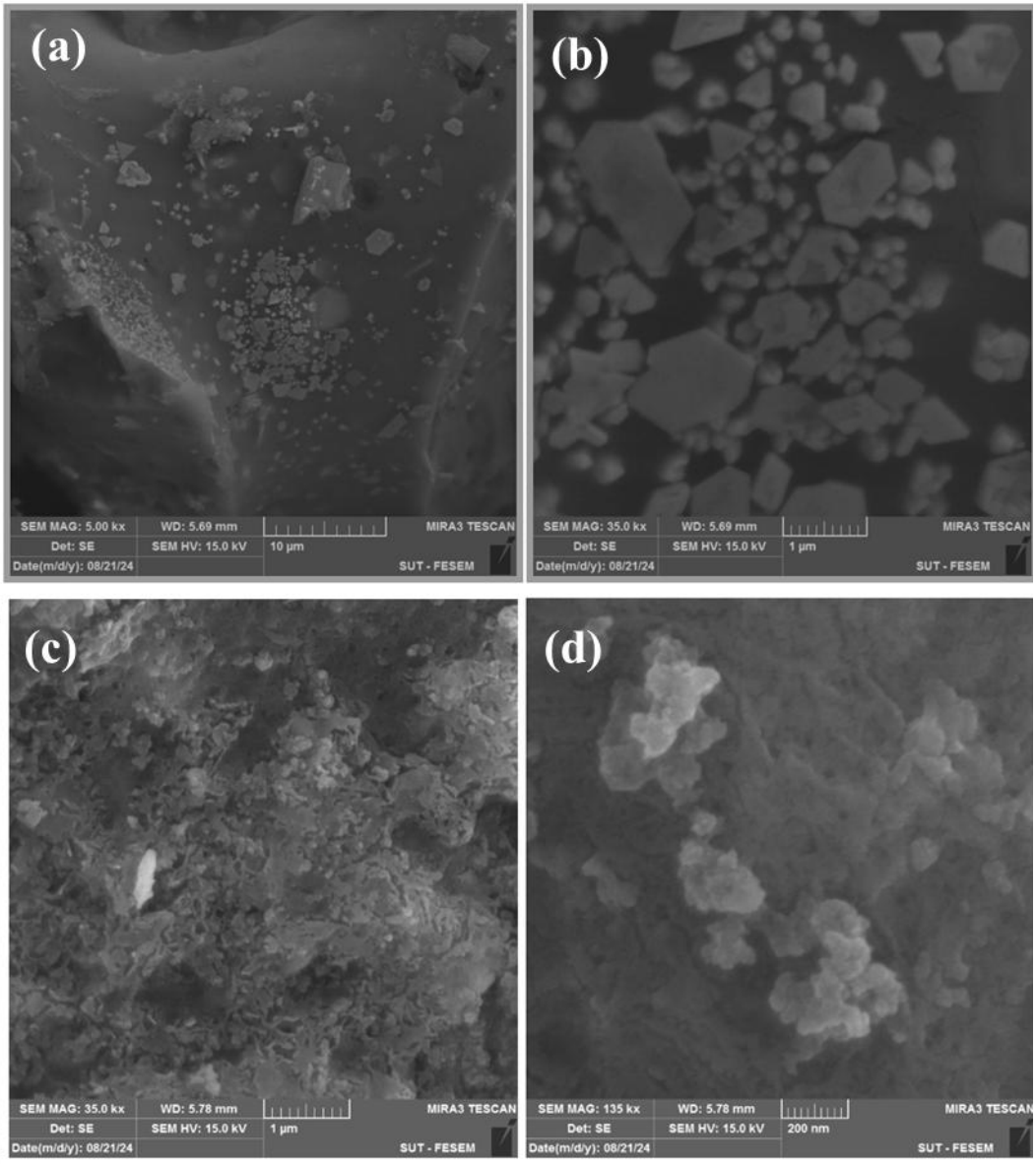

Fig. 4. FESEM image of SA-g-p(AA-IA)/TiO_2 (a, b) before and (c, d) after dye adsorption [43].

42]. These findings align with our prior research on Pb (II) adsorption [43].

The X-ray diffraction (XRD) patterns for both pure TiO_2 and SA-g-p(AA-IA)/TiO_2 nanocomposite (Fig. 3) offer key information about the material's crystal structure. For, TiO_2 (Fig. 3a), the XRD pattern shows distinct and sharp peaks, indicating its crystalline structure. These peaks match the anatase form of TiO_2, known for its high photoactivity. These peaks were observed at 2θ angles around 25.3°, 37.8°, 48.0°, 53.9°, and 62.7°, which correspond to (101), (004), (200), (105), and (204) crystal planes. The sharpness and strength of these peaks confirm that TiO_2 nanoparticles are highly crystalline and pure. When TiO_2 is added to SA-g-p(AA-IA) hydrogel matrix, the XRD pattern changes in several ways (Fig. 3b). The TiO_2 peaks become weaker, since the TiO_2 nanoparticles are dispersed within the non-crystalline polymer matrix. This decrease in peak strength often happens when nanoparticles are embedded and partially covered by a hydrogel network. Some of the characteristic anatase TiO_2 peaks (like at 25.3° for (101) plane) are still visible, showing that the TiO_2 keeps its crystal structure even in nanocomposite. However, these peaks are broader and less intense, suggesting that size of TiO_2 crystals might be slightly smaller, and crystal structure might be distorted due to interactions with polymer's functional groups. The broad peak feature in XRD pattern of nanocomposite (between 15° and 30°) indicates that it is non-crystalline. This confirms that the polymer matrix is mostly amorphous, and TiO_2 is dispersed in polymeric basic [44]. These findings are from our previously reported paper where we studied Pb (II) adsorption from water [43].

FESEM images in Fig. 4 show the nanocomposite's surface after CV dye adsorption. Before adsorption (Fig. 4a), the material has a bumpy and porous surface with visible openings, suggesting a large surface area for dye binding. TiO_2 nanoparticles appear well-dispersed, likely enhancing strength and dye attraction. After dye adsorption (Fig. 4b), the surface becomes noticeably smoother and more densely packed, with most openings filled, confirming that dye molecules have attached. This change from a porous to a smooth surface visually demonstrates the material's strong adsorption capability [42].

Kinetic study

The influence of time (Fig. 5(a, b)) on adsorption of dye by SA-g-p(AA-IA)/TiO_2 hydrogel nanocomposite was investigated by evaluating the adsorption capacity (q_e) and percentage removal (% removal). The results indicated a swift and efficient adsorption process characterized by

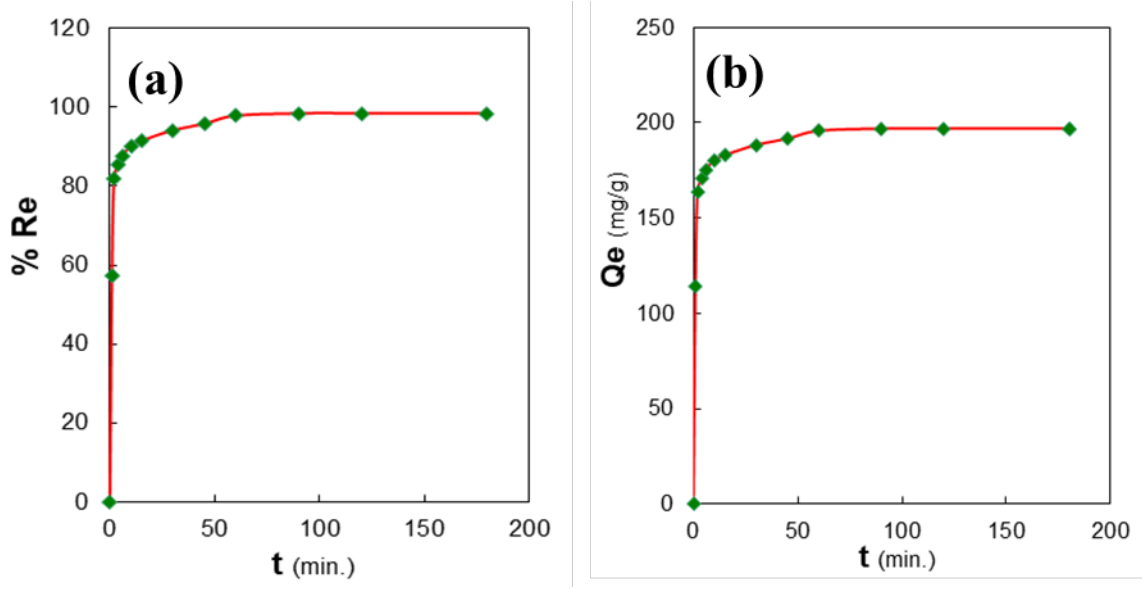

Fig. 5. Effect of time on (a) % removal and (b) adsorption capacity (q_e), mg/g, for CV dye adsorption.

distinct phases. Initially, within the first minute, a q_e of 114.44 mg/g and % removal of 57.22% were observed, signifying rapid dye uptake attributed to abundance of accessible active sites on nanocomposite surface. This was followed by a significant enhancement within the first 10 min, reaching a q_e of 180.33 mg/g and % removal of 90.16%, highlighting a strong initial mass transfer driven by concentration gradient and surface availability. Subsequently, adsorption rate showed a reduction in intermediate phase (10–45 min) due to progressive saturation of active sites. Eventually, the system approached equilibrium in later stages (60–180 min) confirming that equilibrium was attained at 90 min. The minimal change beyond this point suggests adsorption saturation and equilibrium obtained at 90 min [45].

To understand how CV dye is adsorbed onto hydrogel nanocomposite over time, two common kinetic models were applied: pseudo-first-order and pseudo-second-order models. These models help determine the mechanism and slowest step in adsorption process. Pseudo first-order model proposes that rate is related to available number of sites while pseudo second model suggests that the rate-limiting step involves chemical adsorption. Eq. 3 and 4 represents pseudo-first-order and pseudo-second-order model expressions, correspondingly:

$$\log(Q_e - Q_t) = \log Q_e - \frac{k_1}{2.303} t \quad (3)$$

$$\frac{t}{Q_t} = \frac{1}{k_2 Q_e^2} + \frac{t}{Q_e} \quad (4)$$

here, q_t and q_e refers to amounts of dye adsorbed at time t and at equilibrium, respectively (mg/g), while k_1 and k_2 refers to rate constant for pseudo-first (min^{-1}) and second order model (g/mg·min), correspondingly. Results of kinetic study (Fig. 6(a, b) and Table 1 revealed that pseudo-first-order model does not accurately describe how CV dye was adsorbed by nanocomposite due to its

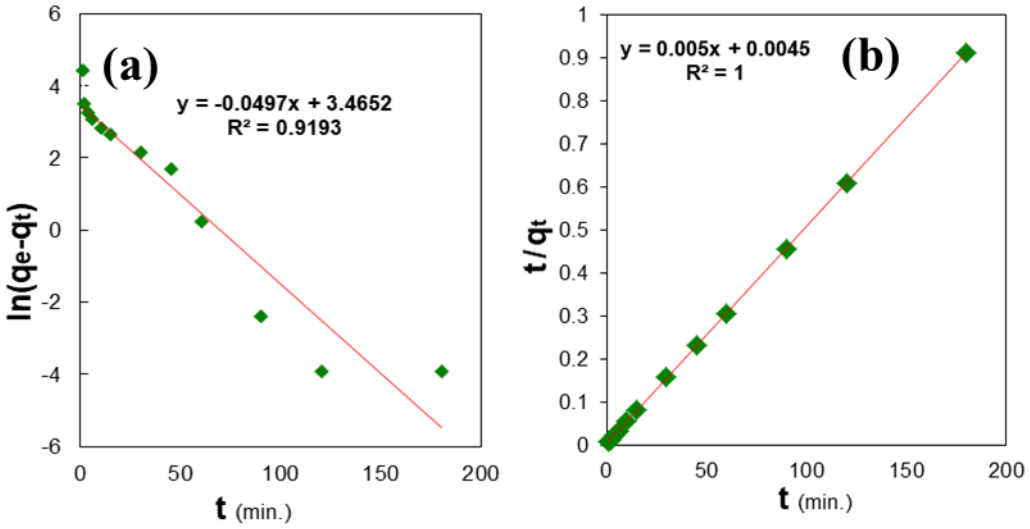

Fig. 6. Graphs for (a) pseudo first and (b) pseudo second order model.

Table 1. Pseudo first and second model parameters. Experimental (mg/g) = 197.07 mg/g.

Model	Pseudo-first order	Pseudo-second order
q_e (mg/g)	31.98	200
R^2 values	0.919	1
Constant	0.049	0.0056
	K_1 (1/min)	K_2 (g/mg · min)

lower regression coefficient value in comparison to pseudo second model. This suggests that process is not primarily controlled by physical diffusion alone. The pseudo-second model provides the best description of kinetics, indicating that chemical adsorption is main mechanism. This likely involves interactions as electrostatic forces, π–π stacking, or H-bonds between CV molecules and functional groups (as –COOH, $–NH_2$) of nanocomposite [46].

Isothermal and temperature study

The adsorption capacity (mg/g) of nanocomposite was increased significantly at higher initial concentrations of CV dye (Fig. 7). Specifically, at a temperature of 10 °C, the adsorption capacities were recorded as 17·92 mg/g at a dye concentration of 10 mg/L, 197·41 mg/g at 100 mg/L, and 928·14 mg/g at 500 mg/L. At 15 °C, q_e values were 17.55 mg/g, 197.15 mg/g, and 919.42 mg/g for the same respective concentrations. When the temperature was raised to 25 °C, the adsorption capacities were 16·45 mg/g, 197·04 mg/g, and 915·76 mg/g. Finally, at 30°C, q_e values were 16.09 mg/g, 192.72 mg/g, and 891.59 mg/g, respectively. These values demonstrate that a high concentration of dye molecules in solution provides a stronger driving force for the movement of dye molecules towards the adsorbent surface and their subsequent attachment. Furthermore, moderate enhancement in temperature, specifically within the range of 10–15 °C, appears to enhance the uptake of the dye by nanocomposite. This enhancement is likely due to the increased kinetic energy of dye molecules and the adsorbent surface, which can facilitate more effective interaction and binding. However, at the highest temperature tested (30 °C), a slight reduction in the adsorption capacity was observed, particularly at higher dye concentrations. This suggests that at elevated temperatures, the equilibrium might shift slightly towards desorption, or that saturation phenomena become more pronounced, limiting further dye uptake [44, 47, 48].

Thermodynamic parameters, including Gibbs free energy (ΔG), enthalpy change (ΔH), and entropy change (ΔS), provide crucial insights into feasibility, spontaneity of adsorption process, as well as the degree of order or disorder at solid–solution interface. Based on the data obtained at 20 °C (from Van't Hoff plot, Fig. 8), the thermodynamic parameters were determined (Table 2) that include ΔG = –5·812 kJ/mol, indicating that the adsorption of CV dye onto nanocomposite is a spontaneous process under these conditions. Further, ΔH is –15.737 kJ/mol, revealing that adsorption process releases heat, and is therefore exothermic. Additionally, ΔS is –34.255 J/mol·K, suggesting a reduction in entropy at the solid–solution interface. This reduction in randomness is likely due to ordering of dye molecules as they become immobilized on specific

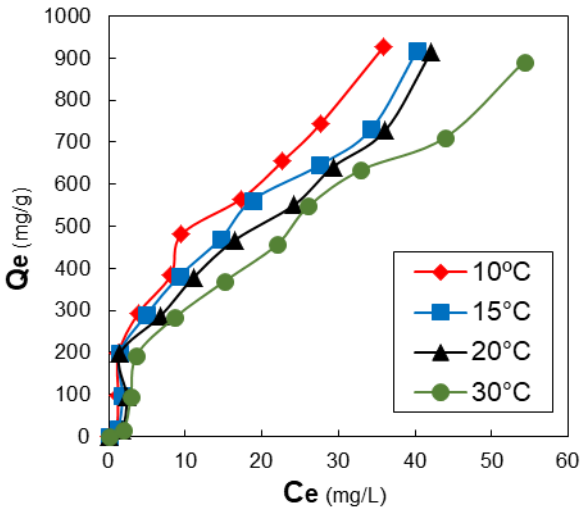

Fig. 7. Effect of dye concentration at different temperatures.

sites of adsorbent surface, thereby reducing their degrees of freedom as compared to their state in the bulk solution [5].

To gain a deeper understanding of the interaction between CV dye molecules and surface of the nanocomposite, three adsorption isotherm models were employed i.e., Langmuir, Freundlich, and Temkin isotherm. Langmuir model (Eq. 5) is based on assumptions of monolayer adsorption, where single layer of adsorbate molecules forms on homogeneous adsorbent surface containing a finite number of identical adsorption sites. Freundlich isotherm (Eq. 6) describes multilayer adsorption on heterogeneous surfaces, where the heat of adsorption varies with the degree of surface coverage. While Temkin model (Eq. 7) takes into account the interactions between adsorbed molecules and assumes that heat of adsorption decreases linearly with surface coverage.

$$\frac{1}{q_e} = \frac{1}{q_{max}} + \frac{1}{q_o b C_e} \quad (5)$$

$$\log q_e = \log K_f + \frac{1}{n}\log C_e \quad (6)$$

$$q_{eq} = B\ln A_T + B\ln C_{eq} \quad (7)$$

where, q_e is equilibrium adsorption capacity, q_{max} is maximum adsorption capacity, K_L is Langmuir constant, Ce is equilibrium dye concentration, K_f is Freundlich constant related to adsorption capacity, 1/n is an empirical parameter related to surface heterogeneity, R is gas constant, T is absolute temperature, b is Temkin constant related to heat of adsorption, and A is Temkin isotherm constant. Isotherm analysis (Fig. 9(a-c)) revealed that the adsorption behaviour can be described by both the Langmuir and Freundlich models (due to their high R^2 values), indicating that the composite surface presents a combination of both energetically uniform sites capable of monolayer adsorption and heterogeneous sites allowing for

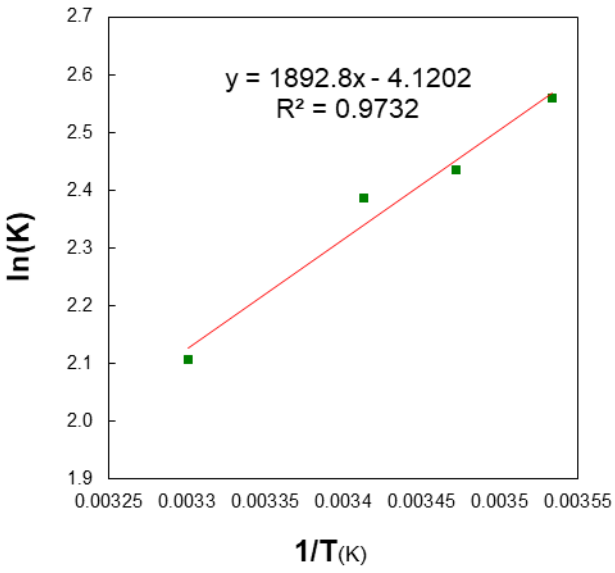

Fig. 8. Van't Hoff plot.

Table 2. Thermodynamic parameters.

T (°C)	ΔG (kJ/mol)	ΔH (kJ/mol)	ΔS (J/mol K)	K_c
20	-5.812	-15.737	-34.255	10.871

multilayer adsorption. The Temkin isotherm also provided insights into the energy of adsorption and adsorbate-adsorbate interactions [49].

Effect of pH and nanocomposite dose

The swelling percentage of SA-g-p(AA-IA)/TiO_2 hydrogel nanocomposite is significantly affected by pH, as the ionic environment influences the charged state of functional groups within its polymer structure and is calculated by Eq. 8:

$$\text{Swelling ratio } (\%) = \frac{W_S - W_d}{W_d} \times 100 \quad (8)$$

The hydrogel's swelling capacity is significantly influenced by pH, as illustrated in Fig. 10a. In acidic conditions, swelling is limited: 130% at pH 2, gradually increasing to 240% at pH 3, and 330% at pH 4. This restricted swelling is due to the protonation of carboxylic (–COOH) and amide groups, which reduces repulsive forces between polymer chains and limits water absorption. As pH increases to 5 and beyond, a substantial enhancement in swelling is observed. Swelling reaches 470% at pH 5, climbing sharply to 670% at pH 6, 850% at pH 7, and peaking at 1060% at pH 8. This significant rise is attributed to the deprotonation of –COOH groups to $–COO^-$, leading to increased electrostatic

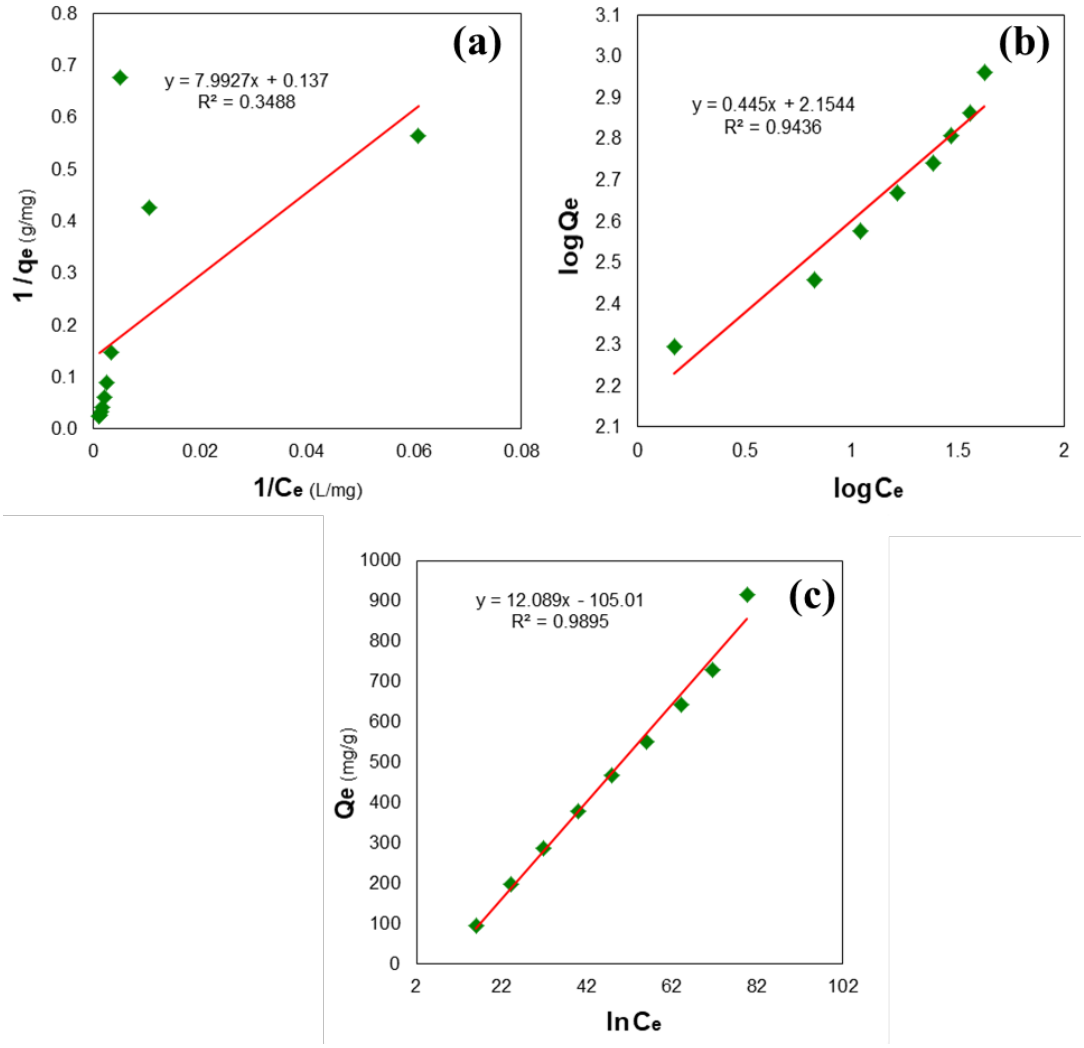

Fig. 9. Graphs for (a) Langmuir, (b) Freundlich and (c) Temkin isotherm models.

repulsion within the polymer network and greater water absorption. Beyond pH 8, swelling continues to increase but at a slower rate, reached 1100% at pH 9, 1120% at pH 10, and stabilized at 1155% at pH 12. This plateau indicates that the ionizable groups are fully deprotonated, and the hydrogel has reached its maximum expansion in alkaline conditions [50]. These findings are consistent with our previous research on Pb (II) adsorption from water [43]. The adsorption capacity of SA-g-p(AA-IA)/TiO_2 hydrogel nanocomposite for CV dye was clearly influenced by pH of solution (Fig. 10b). At a highly acidic pH of 2, the q_e was 195.54 mg/g. This comparatively lower adsorption is likely due to the

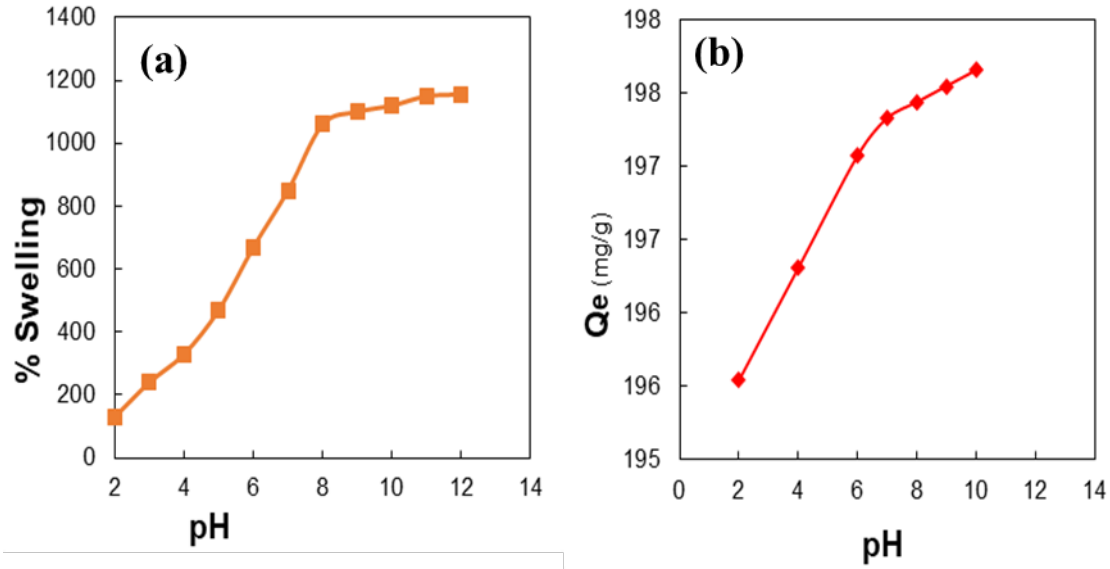

Fig. 10. Effect of pH on (a) swelling ratio and (b) adsorption capacity of nanocomposite for CV dye.

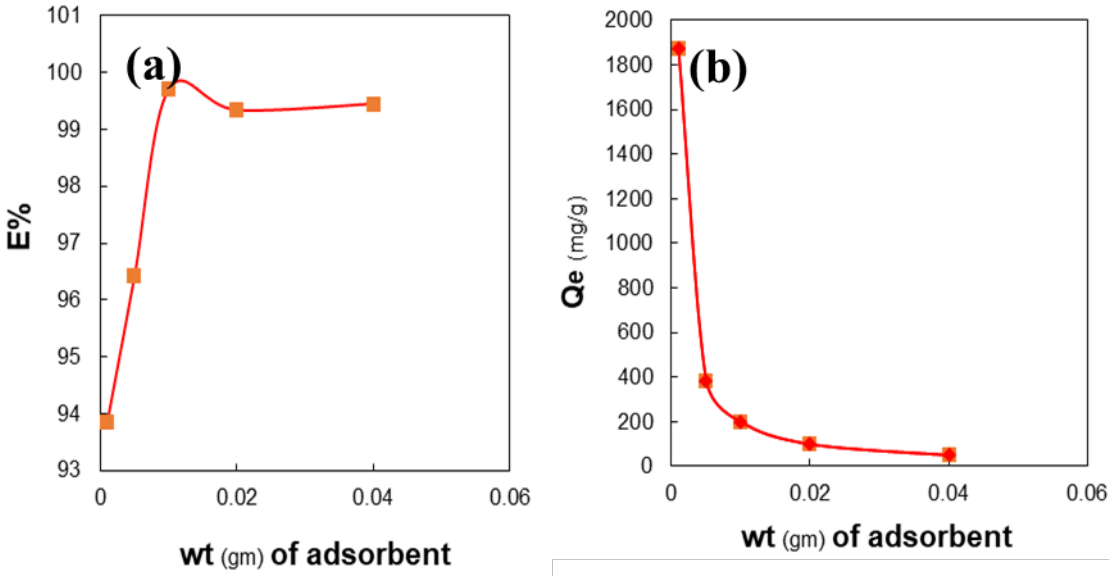

Fig. 11. Effect of nanocomposite dose on (a) % removal and (b) adsorption capacity (q_e), mg/g, for CV dye.

abundance of H^+ ions, which cause protonation of functional groups like $–COO^-$ and –OH on adsorbent surface. This protonation results in a positively charged hydrogel surface, leading to electrostatic repulsion with positively charged dye and consequently reducing its adsorption. As the pH was raised to 4 and then to 6, the adsorption capacity showed improvement, reaching 196.31 mg/g and 197.08 mg/g, respectively. This enhancement can be attributed to gradual loss of protons from the hydrogel's functional groups, imparting more negatively charged active sites that show interactions with cationic dyes. An enhancement in adsorption was observed at pH 7 and 8, where q_e values were 197.33 mg/g and 197.44 mg/g, respectively. Further increasing in pH to 9 and 10 resulted in a slight additional growth in adsorption capacity to 197.55 mg/g and a peak of 197.66 mg/g, indicating that optimal adsorption efficiency is achieved under weakly basic conditions. Beyond this pH, no significant increase in adsorption was observed [50].

Fig. 11(a, b) revealed how different amounts of nanocomposite adsorbent affects both the adsorption capacity and removal efficiency of CV dye. As the quantity of the SA-g-p(AA-IA)/TiO_2 nanocomposite was increased from 0.001 g to 0.01 g, a significant improvement in the percentage of dye removed was observed, rising from 93.84% to 99.70%. This enhancement is attributed to the greater availability of active adsorption sites as more adsorbent material is introduced into the system. However, beyond an adsorbent dose of 0.01 g, the removal efficiency tended to level off, reaching 99.45% at a dose of 0.04 g. This plateau indicates that the majority of the dye present in the solution had been adsorbed. Consequently, further increasing in the adsorbent amount yielded only a minimal improvement in removal. Conversely, the amount of dye adsorbed per unit mass of adsorbent (mg/g) showed a sharp reduction as adsorbent dose was increased. At the lowest dose of 0.001 g, the q_e value was exceptionally high at 1876.78 mg/g, reflecting a large ratio of dye molecules to the amount of adsorbent available. As the dose was increased to 0.005 g and then to 0.01 g, the q_e values decreased to 385.67 mg/g and 199.41 mg/g, respectively. At the highest adsorbent dose of 0.04 g, the adsorption capacity per unit mass fell to only 49.73 mg/g. This trend occurs when a high quantity of adsorbent is added to the system. Furthermore, at higher adsorbent concentrations, the particles may tend to clump together, which can reduce the effective surface area available for adsorption and limit the accessibility of dye molecules to the active sites [50, 51].

CONCLUSION

In this study, a versatile SA-g-p(AA-IA)/TiO_2 hydrogel nanocomposite was successfully created and its performance in removing CV dye from water solutions was assessed. The material displayed desirable structural and surface properties, as confirmed by FTIR, XRD, and FESEM analyses. The adsorption process was significantly affected by operational factors, like notably pH, where basic conditions increased the electrostatic attraction between negatively charged areas and the positively charged dye. Kinetic modeling indicated that the adsorption process adhered to pseudo-second-order kinetics, suggesting a chemical adsorption mechanism. While equilibrium data aligned with both Langmuir and Freundlich isotherm models, indicating the presence of both uniform and varied binding sites. The thermodynamic parameters confirmed that the adsorption was a spontaneous and heat-releasing process. Moreover, the composite showed excellent swelling capabilities and high removal efficiency (exceeding 99.7 %) even with a small amount of adsorbent. These results strongly suggest that the SA-g-p(AA-IA)/TiO_2 hydrogel nanocomposite presents a significant potential as an affordable, effective, and environmentally friendly adsorbent for treating industrial wastewater contaminated with cationic dyes.

CONFLICT OF INTEREST

The authors declare that there is no conflict of interests regarding the publication of this manuscript.

REFERENCES

1. Mekonnen BY, Abate GYA, Mekonnen SD, Gebeyehu AG. Adsorption of methylene blue dye onto acid-treated tej residue: Kinetic, equilibrium and thermodynamic study. Indian Journal of Chemical Technology (IJCT). 2023;30(1):94-102.
2. Liyanaarachchi H, Thambiliyagodage C, Lokuge H, Vigneswaran S. Kinetics and thermodynamics study of methylene blue adsorption to sucrose-and urea-derived nitrogen-enriched, hierarchically porous carbon activated by KOH and H3PO4. ACS omega. 2023;8(18):16158-16173.
3. Khliwi FS, Alshamsi HA. Design of a Z-Scheme System with g-C_3N_4/WO_3/$ZnFe_2O_4$ Nanocomposite for Photocatalytic

Degradation of Rhodamine B. J Cluster Sci. 2025;36(3).
4. SATTAR ODA, KHALID RM, YUSOFF SFM. Optimizing Methylene Blue Dye Adsorption onto Liquid Natural Rubber-Based Hydrogel: Kinetics, Isotherms and Reusability. Sains Malaysiana. 2024;53(5):1149-1166.
5. Batool M, Javed T, Wasim M, Zafar S, Din MI. Exploring the usability of Cedrus deodara sawdust for decontamination of wastewater containing crystal violet dye. Desalination and Water Treatment. 2021;224:433-448.
6. Ghorbi MD, Qasim MJ, Kadhum AAH, Othman MAM, Dehghani A, Ghaffariyan S, et al. An ecological assessment of global thyroid cancer incidence and mortality according to the human development index in 2020. Journal of Parathyroid Disease. 2025;13(1).
7. Ali MM, Mhaibes RM, Othman MAM, Lahhob QR, Qasim MJ. Association between triglyceride-glucose index and risk of chronic kidney disease: a systematic review and meta-analysis. Journal of Nephropharmacology. 2024;13(2).
8. Sadeghi M. Synthesis of a biocopolymer carrageenan-g-poly (AAm-co-IA)/montmorilonite superabsorbent hydrogel composite. Brazilian Journal of Chemical Engineering. 2012;29:295-305.
9. Hussain NA, Jasim LS. Synthesis and Characterization of Kappa (κ)-Carrageenan-grafted poly (acrylic acid-co-itaconic acid)/Multi-walled Carbon Nanotube (κC-g-poly (AAC-co-IA)/MWCNT) Composite for Removing Safranin-O Dye from Aqueous Solution. Process Saf Environ Prot. 2025:106828.
10. AlSaadi EK, Darweesh MA, Al Jawadi HF, Othman MAM. Demographic Characteristics, Clinical Features, Laboratory, and Radiological Findings in Children Admitted to COVID19 Center in Amara City, Misan Province, Iraq. Journal of Medicinal and Chemical Sciences. 2023;6(1):34-43.
11. Hmood NA, Othman MAM, Ali MM. Transcription factor 7-like 2 gene polymorphisms rs7903146associationwith type 2 diabetic polycystic ovarian syndrome women of Iraqi Population. Annals of Tropical Medicine and Public Health. 2019;22(12).
12. Majeed HJ, Idrees TJ, Mahdi MA, Abed MJ, Batool M, Yousefi SR, et al. Synthesis and application of novel sodium carboxy methyl cellulose-g-poly acrylic acid carbon dots hydrogel nanocomposite (NaCMC-g-PAAc/ CDs) for adsorptive removal of malachite green dye. Desalination and Water Treatment. 2024;320.
13. Javed T, Thumma A, Uddin AN, Akhter R, Babar Taj M, Zafar S, et al. Batch adsorption study of Congo Red dye using unmodified Azadirachta indica leaves: isotherms and kinetics. Water Practice and Technology. 2024;19(2):546-566.
14. Sharma S, Sharma G, Kumar A, AlGarni TS, Naushad M, ALOthman ZA, et al. Adsorption of cationic dyes onto carrageenan and itaconic acid-based superabsorbent hydrogel: Synthesis, characterization and isotherm analysis. J Hazard Mater. 2022;421:126729.
15. Taher A, Jasim LS, Mehmood Z, Zawar MD, Haider MN, Batool M. Applications of Nano Composites for Heavy Metal Removal from Water by Adsorption: Mini Review. Journal of Nanostructures. 2024;14(4):1239-1251.
16. Urooj H, Javed T, Taj MB, Nouman Haider M. Adsorption of crystal violet dye from wastewater on Phyllanthus emblica fruit (PEF) powder: kinetic and thermodynamic. Int J Environ Anal Chem. 2024;104(19):7474-7499.
17. Zeeshan M, Javed T, Kumari C, Thumma A, Wasim M, Taj MB, et al. Investigating the Interactions between Dyes and Porous/Composite Materials: A Comprehensive Study. Sustainable Chemistry for the Environment. 2025:100217.
18. Bukhari A, Javed T, Haider MN. Adsorptive exclusion of crystal violet dye from wastewater by using fish scales as an adsorbent. J Dispersion Sci Technol. 2023;44(11):2081-2092.
19. Imran MS, Javed T, Areej I, Haider MN. Sequestration of crystal violet dye from wastewater using low-cost coconut husk as a potential adsorbent. Water Sci Technol. 2022;85(8):2295-2317.
20. Javed T, Ghzal Q, Zghair AN, Haider MN, Abed MJ, Jasim LS, et al. Sustainable Dye Wastewater Treatment: A Review of Effective Strategies and Future Directions. Physical Chemistry Research. 2025.
21. Shah A, Arjunan A, Thumma A, Zakharova J, Bolarinwa T, Devi S, et al. Adsorptive removal of arsenic from drinking water using KOH-modified sewage sludge-derived biochar. Cleaner Water. 2024;2:100022.
22. Jamel HO, Jasim MH, Mahdi MA, Ganduh SH, Batool M, Jasim LS, et al. Adsorption of Rhodamine B dye from solution using 3-((1-(4-((1H-benzo[d]imidazol-2-yl)amino) phenyl)ethylidene)amino)phenol (BIAPEHB)/ P(AA-co-AM) composite. Desalination and Water Treatment. 2025;321.
23. Salunkhe B, Schuman TP. Super-adsorbent hydrogels for removal of methylene blue from aqueous solution: dye adsorption isotherms, kinetics, and thermodynamic properties. Macromol. 2021;1(4):256-275.
24. Alzayd AAM, Zghair AN, Essa AM, Jawad AS, Abed MJ, Batool M, et al. Isotherm and Thermodynamic Analysis of Azur C Dye Adsorption on GO/P (CMC-Co-Am) Nanocomposite. Journal of Nanostructures. 2024;14(3):845-856.
25. Van Tran V, Park D, Lee Y-C. Hydrogel applications for adsorption of contaminants in water and wastewater treatment. Environmental Science and Pollution Research. 2018;25:24569-24599.
26. Hamid MM, Shahad RF, Almekh MTA. Assessment of Groundwater Quality and Suitability for Irrigation Purpose in Northern Babil Governorate. Journal of Environmental and Earth Sciences. 2025;7(4):368-377.
27. Shahad RF, Hamid MM. Impact of Bentonite and Humic Acid on the Growth and Flowering of Catharanthus roseus L. in Sandy Soil. Journal of Environmental and Earth Sciences. 2025;7(1):157-166.
28. Al-Suraify SMT, Hussien LB. Synthesis and characterization of new compounds derived from 1H-indol-5-ylamine. Applied Nanoscience (Switzerland). 2023;13(3):2083-2092.
29. Shahad RF, Abdullah AM, Essa SK. Studying the Effect of Agriculturally Exploited Soils on the Transformation of Mica Minerals using Infrared Spectroscopy (IR). Malaysian Journal of Chemistry. 2021;23(4):144-153.
30. Mhammed AAA, Zghair AN, Essa AM, Jawad AS, Abed MJ, Batool M, et al. Isotherm and Thermodynamic Analysis of Azur C Dye Adsorption on GO/P(CMC-Co-Am) Nanocomposite. Journal of Nanostructures. 2024;14(3):845-856.
31. Taher AM, Jasim LS, Mehmood Z, Zawar MD, Haider MN, Batool M. Applications of Nano Composites for Heavy Metal Removal from Water by Adsorption: Mini Review. Journal of Nanostructures. 2024;14(4):1239-1251.
32. Abdulsahib WK, Sahib HH, Mahdi MA, Jasim LS. Adsorption Study of Cephalexin Monohydrate Drug in Solution on Poly (vinyl pyrrolidone-acryl amide) Hydrogel Surface. International Journal of Drug Delivery Technology.

2021;11(4):1169-1172.
33. Aljeboree AM, Alkaim AF. Studying removal of anionic dye by prepared highly adsorbent surface hydrogel nanocomposite as an applicable for aqueous solution. Sci Rep. 2024;14(1):9102.
34. Arshad R, Javed T, Thumma A. Exploring the efficiency of sodium alginate beads and Cedrus deodara sawdust for adsorptive removal of crystal violet dye. J Dispersion Sci Technol. 2024;45(12):2330-2343.
35. Guo H, Jiao T, Zhang Q, Guo W, Peng Q, Yan X. Preparation of graphene oxide-based hydrogels as efficient dye adsorbents for wastewater treatment. Nanoscale research letters. 2015;10:1-10.
36. Aljeboree AM, Radia ND, Jasim LS, Alwarthan AA, Khadhim MM, Salman AW, et al. Synthesis of a new nanocomposite with the core TiO_2/hydrogel: Brilliant green dye adsorption, isotherms, kinetics, and DFT studies. Journal of Industrial and Engineering Chemistry. 2022;109:475-485.
37. Lučić M, Milosavljević N, Radetić M, Šaponjić Z, Radoičić M, Krušić MK. The potential application of TiO2/hydrogel nanocomposite for removal of various textile azo dyes. Sep Purif Technol. 2014;122:206-216.
38. Javed T, Kausar F, Zawar MD, Khalid N, Thumma A, Ismail A, et al. Investigating the adsorption potential of coconut coir as an economical adsorbent for decontamination of lanthanum ion from aqueous solution. J Dispersion Sci Technol. 2024.
39. Pang YL, Tee SF, Limg S, Abdullah AZ, Ong HC, Wu C-H, et al. Enhancement of photocatalytic degradation of organic dyes using ZnO decorated on reduced graphene oxide (rGO). Desalination and Water Treatment. 2018;108:311-321.
40. Mannan HA, Nadeem R, Bibi S, Javed T, Javed I, Nazir A, et al. Mesoporous activated TiO_2/based biochar synthesized from fish scales as a proficient adsorbent for deracination of heavy metals from industrial efflux. J Dispersion Sci Technol. 2022:1-13.
41. Faleh YA, Radhy ND, editors. Removal of Metformin hydrochloride from Aqueous Solutions by using Carboxymethyl cellulose-g-poly (acrylic acid-co-acrylamide) Hydrogel: Adsorption and Thermodynamic Studies. IOP Conference Series: Earth and Environmental Science; 2021: IOP Publishing.
42. Thakur S, Arotiba OA. Synthesis, swelling and adsorption studies of a pH-responsive sodium alginate–poly (acrylic acid) superabsorbent hydrogel. Polym Bull. 2018;75:4587-4606.
43. Mutashar MO, Shahad RF, Jasim IS, Batool M. Removal of Pb (II) Ions from Water by Adsorption on Sodium Alginate-g-poly (Acrylic acid-co-Itaconic acid)/Titanium Dioxide [SA-gp (AA-IA)/TiO2] Hydrogel Nanocomposite. Journal of Nanostructures. 2025;15(3):983-996.
44. Al-Asadi ST, Mussa ZH, Al-Qaim FF, Kamyab H, Al-Saedi HFS, Deyab IF, et al. A Comprehensive Review of Methylene Blue Dye Adsorption on Activated Carbon from Edible Fruit Seeds: A Case Study on Kinetics and Adsorption Models. Carbon Trends. 2025:100507.
45. A Mahdi M, Jasim LS, O Jamel H. Removal of Rhodamine B from Aqueous Solutions Using Chitosan-g-poly (acrylic acid)/2-(((1E, 2E)-1, 2-diphenyl-2-((4 (E-1-(thiazol 2ylimino) ethyl) phenyl) imino) ethylidene) amino) phenol composite as an Adsorbent. Journal of Nanostructures. 2023.
46. Abdullah AR, Jasim LS. High-efficiency removal of diclofenac sodium (DS) drug using chitosan-grafted-poly (acrylic acid-co-N-isopropylacrylamide)/kaolin clay hydrogel composite. Int J Environ Anal Chem. 2024:1-21.
47. Atyaa AI, Jasim LS, Jamel HO. Synthesis and Characterization of Biapehb/P(Aa-Co-Am)) Composites Hydrogels and their Kinetic Study as Adsorbent for Rhodamine 6g Dye from their Aqueous Solutions International Journal of Drug Delivery Technology. 2022;12(1):316-319.
48. Bukhari A, Javed T, Haider MN. Adsorptive exclusion of crystal violet dye from wastewater by using fish scales as an adsorbent. J Dispers Sci Technol. 2022:1-12.
49. Rafak SH, Jasim LS. Synthesis of novel bentonite/pectin-grafted-poly (crotonic acid-co-acrylic acid) hydrogel nanocomposite for adsorptive removal of safranin O dye from aqueous solution. Int J Environ Anal Chem. 2024:1-24.
50. Rehman H, Javed T, Thumma A, Uddin AN, Singh N, Baig MM, et al. Potential of easily available low-cost raw cotton for the elimination of methylene blue dye from polluted water. Desalination and Water Treatment. 2024;318:100319.